A fast radio burst associated with a Galactic magnetar

https://doi.org/10.1038/s41586-020-2872-x

Received: 12 May 2020

Accepted: 21 September 2020

Published online: 4 November 2020

Check for updates

C. D. Bochenek[1,2]✉, V. Ravi[2], K. V. Belov[3], G. Hallinan[2], J. Kocz[2,4], S. R. Kulkarni[2] & D. L. McKenna[5]

Since their discovery in 2007[1], much effort has been devoted to uncovering the sources of the extragalactic, millisecond-duration fast radio bursts (FRBs)[2]. A class of neutron stars known as magnetars is a leading candidate source of FRBs[3,4]. Magnetars have surface magnetic fields in excess of 10^{14} gauss, the decay of which powers a range of high-energy phenomena[5]. Here we report observations of a millisecond-duration radio burst from the Galactic magnetar SGR 1935+2154, with a fluence of 1.5 ± 0.3 megajansky milliseconds. This event, FRB 200428 (ST 200428A), was detected on 28 April 2020 by the STARE2 radio array[6] in the 1,281–1,468 megahertz band. The isotropic-equivalent energy released in FRB 200428 is 4×10^3 times greater than that of any radio pulse from the Crab pulsar—previously the source of the brightest Galactic radio bursts observed on similar timescales[7]. FRB 200428 is just 30 times less energetic than the weakest extragalactic FRB observed so far[8], and is drawn from the same population as the observed FRB sample. The coincidence of FRB 200428 with an X-ray burst[9–11] favours emission models that describe synchrotron masers or electromagnetic pulses powered by magnetar bursts and giant flares[3,4,12,13]. The discovery of FRB 200428 implies that active magnetars such as SGR 1935+2154 can produce FRBs at extragalactic distances.

Three 1,281–1,468 MHz radio detectors comprise STARE2 (ref. [6]) and are located across the southwestern United States. All three detectors were triggered by an event originally named ST 200428A—and here referred to by its International Astronomical Union designation, FRB 200428—at an Earth-centre arrival time of 28 April 2020 14:34:24.45481(3) UTC at infinite frequency (standard errors are reported with the last significant figures in parenthesis; UTC, coordinated universal time). The dynamic spectrum of FRB 200428 is shown in Fig. 1. The detected signal-to-noise ratios (S/N) were 21, 15 and 20 (see Methods). The burst had a dispersion measure (DM) of 332.702(8) pc cm^{-3} and and a band-averaged fluence of $1.5(3) \times 10^6$ Jy ms (see Table 1). The full-width at half-maximum (FWHM) temporal width of the burst, after correcting for propagation and instrumental effects (see Methods), is 0.61(9) ms. Although we modelled the temporal profile of the burst that is intrinsic to the source as a Gaussian, it is possible that there is unresolved substructure on timescales shorter than the instrumental resolution of 0.122 ms.

On 27 April 2020, the Swift Burst Alert Telescope reported multiple bursts from the soft-γ-ray repeater (SGR) SGR 1935+2154 (ref. [14]). One day later, the CHIME/FRB collaboration reported a burst of approximately 10^3 Jy ms in the 400–800 MHz band from the approximate direction of SGR 1935+2154 (Fig. 2)[15]. We expedited our daily inspection of STARE2 triggers and found an event that was detected at approximately the same time and DM as the CHIME event, but with a fluence roughly 1,000 times higher. The localization region of FRB 200428 includes SGR 1935+2154 (Fig. 2). Shortly thereafter, a constellation of space-borne instruments[9–11] reported a 1-s-long X-ray (1–250 keV) burst from the direction of SGR 1935+2154. INTEGRAL determined that the burst was coming from within 5.5 arcmin of the SGR within seconds of the burst. This X-ray burst occurred at precisely the same time as the CHIME bursts and FRB 200428, after accounting for the dispersion delay and different spatial positions of the observatories (Fig. 1). On 30 April 2020, the Five hundred meter Aperture Spherical Telescope (FAST) detected[16] a weak (0.06 Jy ms) burst in the 1.02–1.48 GHz band and localized it to within 3 arcmin (the size of the FAST beam) of SGR 1935+2154. The DM links the CHIME, STARE2 and FAST bursts with the best localization proved by FAST. The temporal coincidence of the CHIME, STARE2 and X-ray bursts then link FRB 200428 to SGR 1935+2154.

Observational classification

The fluence of FRB 200428 is unprecedented for a neutron star. Using a distance of 9.5 kpc (see refs. [17–19]) we infer an isotropic-equivalent energy release of $2.2(4) \times 10^{35}$ erg and a spectral energy release of $1.6(3) \times 10^{26}$ erg Hz^{-1} (see Methods). Previously, giant radio pulses (GRPs) from pulsars[20] were the brightest known sources of Galactic radio pulses. GRPs are emitted stochastically amongst regular radio pulses but have sub-microsecond durations, in contrast to the millisecond duration of the observed FRBs, including FRB 200428. The brightest and most luminous GRP detected so far was observed at 430 MHz from the Crab pulsar and had a fluence of 3×10^4 Jy ms and

[1]Cahill Center for Astronomy and Astrophysics, California Institute of Technology, Pasadena, CA, USA. [2]Owens Valley Radio Observatory, California Institute of Technology, Pasadena, CA, USA. [3]Jet Propulsion Laboratory, California Institute of Technology, Pasadena, CA, USA. [4]Department of Astronomy, University of California, Berkeley, CA, USA. [5]Caltech Optical Observatories, California Institute of Technology, Pasadena, CA, USA. ✉e-mail: cbochenek@astro.caltech.edu

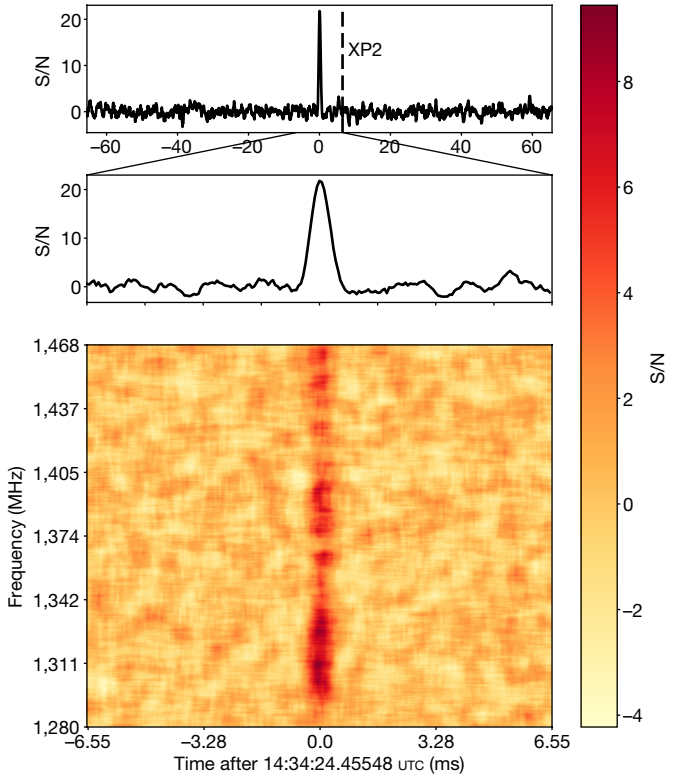

Fig. 1 | Time series and dynamic spectrum of FRB 200428. *S/N* values obtained from the Owens Valley Radio Observatory (OVRO) alone. The quoted times are relative to the Earth-centre arrival time of the burst at infinite frequency. For a description of the data processing, see Methods. Top, de-dispersed time series of all available data on FRB 200428 (see Methods). The original data were de-dispersed at DM = 332.702 pc cm^{-3}. We detect no other radio bursts in our data, which span a window of 131.072 ms (the total amount of data stored around this event) centred on the time of FRB 200428. We place an upper limit of <400 kJy ms on bursts with $S/N > 5$ in this time window. The relative arrival time of the second, brighter peak in the coincident X-ray burst (XP2) is indicated as a vertical dashed line[9,11]. The full X-ray burst lasted approximately 1 s centred on 14:34:24.444 UTC (arrival time at the Earth centre). Middle, expanded plot of the region surrounding the burst. Bottom, dynamic spectrum of FRB 200428 corrected for the effects of dispersion.

Table 1 | Data on FRB 200428

Property	Measurement
OVRO arrival time at ν = 1,529.267578 MHz	28 April 2020 14:34:25.02657(2) UTC
OVRO arrival time at $\nu = \infty$[a]	28 April 2020 14:34:24.43627(3) UTC
Earth centre arrival time at $\nu = \infty$[a]	28 April 2020 14:34:24.45548(3) UTC
Fluence (MJy ms)	1.5(3)
Dispersion measure, DM (pc cm^{-3})	332.702(8)
Intrinsic burst FWHM[b] (ms)	0.61(9)
Isotropic-equivalent energy release[c] (erg)	$2.2(4) \times 10^{35}$

Standard errors in the final significant figures (68% confidence) are given in parentheses.
[a]The correction to the infinite-frequency ($\nu = \infty$) arrival time is carried out using the DM quoted in this table, and assuming a dispersion constant of $(1/2.41) \times 10^4$ s MHz^2 pc^{-1} cm^3 (ref. [31]).
[b]FWHM of the Gaussian used to model the intrinsic burst structure (Methods).
[c]This assumes a distance to SGR 1935+2154 of 9.5 kpc.

an isotropic-equivalent energy release of 6×10^{31} erg (ref. [7]). FRB 200428 is therefore a factor of approximately 4×10^3 more energetic than any millisecond radio burst previously observed from a source within the Milky Way.

From Fig. 3, we see that FRB 200428 is most plausibly related to FRBs observed at extragalactic distances. FRBs span a wide range of energies, but the least energetic FRB reported so far (FRB 180916.J0158+65) had an isotropic-equivalent spectral energy of just $5(2) \times 10^{27}$ erg Hz^{-1} at 1.7 GHz (ref. [8]). Using the parameters from Table 1, the brightness temperature of FRB 200428 is approximately 1.4×10^{32} K, consistent with those of FRBs[2]. Since the first announcement of their detection of FRB 200428, the CHIME/FRB collaboration revised the flux and fluence of FRB 200428 (ref. [21]). The factor-of-seven disparity, which is probably intrinsic, between the fluence of FRB 200428 and that of the CHIME event is consistent with previous wide-band radio observations of FRBs[22].

We observed no other FRB-like radio bursts besides FRB 200428 during 448 days of observing. STARE2 has a detection threshold of 300 kJy for millisecond-duration bursts within a field of view of 1.84 sr, which corresponds to the beamwidth of 3 dB (see Methods). We observed no other radio bursts from SGR 1935+2154, despite the occurrence of 79 X-ray bursts visible to STARE2 (see Methods).

Based on the entire STARE2 observing campaign, for bursts with energy releases equal to or greater than that of FRB 200428 we derive a volumetric rate of $7^{+9}_{-6} \times 10^7$ Gpc^{-3} yr^{-1}, where 1σ uncertainties are quoted (as throughout). At 95% confidence, the volumetric rate is $>4 \times 10^6$ Gpc^{-3} yr^{-1}. This rate is consistent with an extrapolation of the luminosity function of bright FRBs (see Methods).

SGR 1935+2154 is located approximately 100 pc above the plane of the Milky Way disk and situated at the centre of a known supernova remnant[17]. Such a locale is consistent with those of six of the seven accurately localized FRBs within their host galaxies[8,23–26]. These six host galaxies are similar to the Milky Way in their masses and star-formation rates. There is no evidence for a large DM enhancement locally to SGR 1935+2154 (see Methods). The Faraday rotation measure of the weak radio pulse detected by FAST from SGR 1935+2154 is consistent with the rotation measure of radio emission from the associated supernova remnant at the position of SGR 1935+2154 (ref. [17]), implying no significant enhancement in the plasma magnetization that immediately surrounds the SGR.

Implications for FRBs

We have established that FRB 200428 is arguably drawn from the same population as the observed FRB sample; this implies that magnetars such as SGR 1935+2154 are viable FRB engines. However, it is puzzling that events like FRB 200428 have not previously been observed from SGR 1935+2154 or from any of the 30 known magnetars in the Milky Way[5], especially given that SGR 1935+2154 is not extraordinary in its spin period or magnetic field compared to other Galactic magnetars. This may be due to the fact that bursts of this brightness are often flagged as radio frequency interference or saturate receivers. Furthermore, the X-ray burst coincident with FRB 200428 (isotropic-equivalent energy release of $8.3(8) \times 10^{39}$ erg) was a typical example of a magnetar burst[5], with perhaps some unusual spectral characteristics[11]. So apparently, only a subset of X-ray bursts are accompanied by bright radio emission.

The properties of FRB 200428 and the rarity of similar events provide insight into the emission mechanism of FRBs. The temporal coincidence of FRB 200428 with an X-ray burst is not fully consistent with models in which FRB emission is generated within the magnetospheres of magnetars. If the X-ray burst is emitted through standard mechanisms, magnetospheric FRB emission is predicted to occur immediately before the X-ray bursts[27]. Indeed, X-ray bursts appear to suppress magnetospheric radio emission from the magnetar-like pulsar PSR J1119-6127 for several tens of seconds[28].

The energetics of FRB 200428 and its coincident X-ray burst are consistent with some models for FRB emission from beyond the

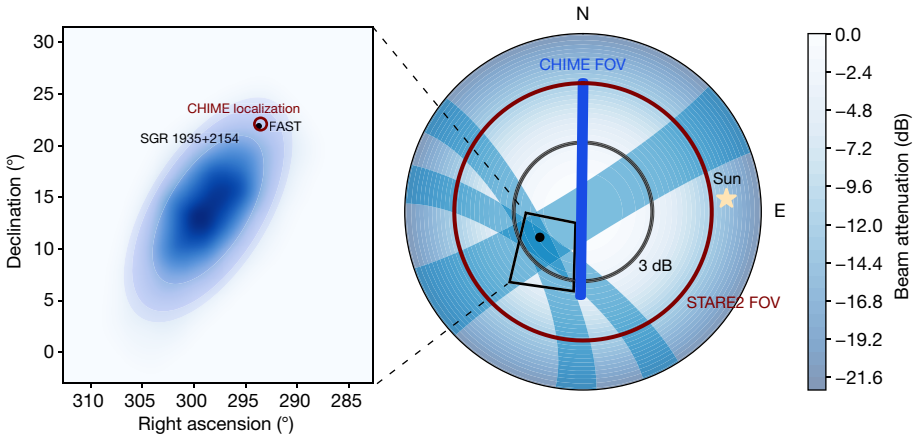

Fig. 2 | STARE2 localization of FRB 200428. Right, altitude and azimuth view of the sky at the OVRO STARE2 station at the time when FRB 200428 was detected. The maroon circle corresponds to the STARE2 field of view (FOV), which is set by the edge of a horizon shield at OVRO[6]. The black circle labelled '3 dB' indicates the zenith angle corresponding to the FWHM of the STARE2 response on the sky. The thick blue line represents the CHIME FOV. The star denotes the Sun, which is a common source of STARE2 triggers[6]. The black dot represents the known position of SGR 1935+2154. The three light-blue arcs correspond to the 95%-confidence localizations for each individual STARE2 baseline. The black quadrilateral represents the outline of the region shown in the left panel. Left, from the centre outwards, the ellipses represent the 68.4%-, 90%- and 95%-confidence STARE2 localization regions of FRB 200428. The blue gradient corresponds to the probability that the burst occurred at that location. The CHIME localization region[21] corresponds approximately to the maroon circle. The known position of SGR 1935+2154, which is identical to the position of the weak burst detected by FAST[16], is shown as a black dot.

magnetospheres of magnetars. Models for FRB emission external to magnetospheres have been developed only for the most energetic X- and γ-ray bursts from magnetars, known as giant flares. An event that manifests as a giant flare is also predicted to result in the ejection of a highly magnetized portion of the magnetar magnetosphere at relativistic speeds, known as a 'plasmoid'. Although plasmoids are distinct from the observed X- and γ-ray radiation from giant flares, they are expected to contain comparable amounts of energy ($>10^{44}$ erg)[3,4,12]. An FRB radiated by the synchrotron maser mechanism may result from a shock driven by the plasmoid into the external medium[3,4,12]. Alternatively, the plasmoid may trigger an electromagnetic pulse just beyond the magnetosphere, resulting in an FRB[13]. FRB energies of $10^{-7}E_{pl}$–$10^{-4}E_{pl}$, where E_{pl} is the energy of the plasmoid, are predicted by these models. The ratio between the radio energy release of FRB 200428 and the X-ray energy release of the coincident burst is approximately 3×10^{-5}, consistent with these predictions for the energy of the radio burst.

In this scenario, individual X-ray bursts from magnetars would result in radio emission being relativistically beamed in random directions, explaining the rarity of events like FRB 200428. However, it remains to be seen whether the theory developed for plasmoids launched by giant magnetar flares can be extended to lower-energy events such as the 10^{40}-erg X-ray burst coincident with FRB 200428. The close coincidence between FRB 200428 and the associated X-ray burst (Fig. 1) is difficult to explain if the FRB were launched extremely far from the magnetosphere[4], unless the X-ray emission was not associated with the FRB-emitting region.

Our observations suggest that magnetars such as those observed in the Milky Way can produce FRBs. We estimate that the volumetric rate of events like FRB 200428 is consistent with a low-energy extrapolation of the FRB volumetric rate[29]. This suggests that we have observed the dominant FRB channel. However, it is by no means proven that magnetars can produce the highest-luminosity FRBs. There may be other surprises, such as the discovery of FRBs from galaxies lacking star formation. The link between SGRs and FRBs and the large inferred rate of low-luminosity FRBs implied by the detection of FRB 200428 provide motivation for dedicated radio burst searches from nearby, rapidly star-forming galaxies such as Messier 82, which has a star-formation rate more than 10 times that of the Milky Way[30].

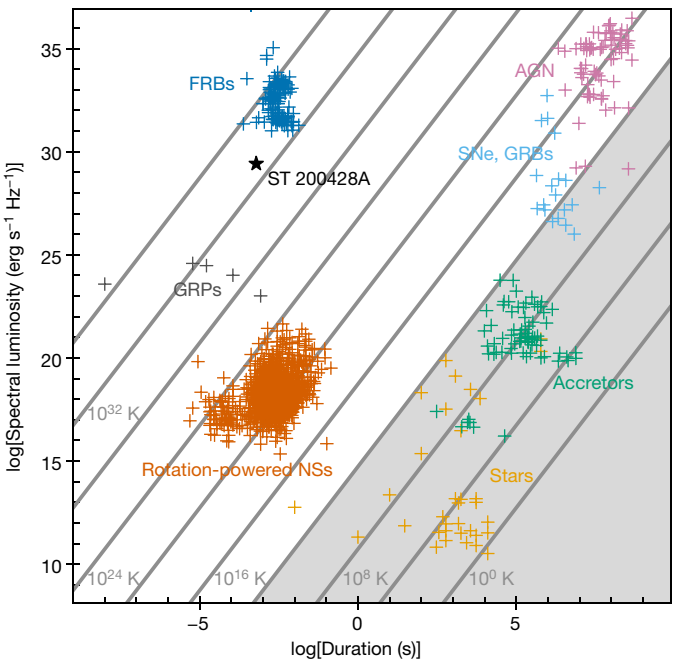

Fig. 3 | Phase space of centimetre-wavelength radio transient events. The vertical extent of the FRB 200428 star corresponds to the uncertainty in the spectral luminosity caused by the uncertain distance to SGR 1935+2154, which ranges between 6.5 and 12.5 kpc (refs. [17–19]). Only isotropic-equivalent spectral luminosities are shown. The FRBs plotted include only bursts detected in 1–2 GHz from sources at known distances. All other data are from refs. [32,33]. 'GRPs' denotes giant radio pulses; 'rotation-powered NSs' refers to rotating radio transients and rotation-powered pulsars; 'accretors' indicates accreting binary systems in the Milky Way, 'SNe' and 'GRBs' refers to supernovae and γ-ray bursts at extragalactic distances, respectively, and 'AGN' denotes accreting supermassive black holes. All radio transients plotted are detections in the range 1–2 GHz. Lines of constant brightness temperature at a reference frequency of 1.4 GHz are shown, and the shaded area (representing brightness temperatures lower than 10^{12} K) indicates sources that are likely incoherent emitters that are not relativistically boosted. The spectral luminosity of FRB 200428 was derived by dividing the burst spectral energy by the duration.

Online content

Any methods, additional references, Nature Research reporting summaries, source data, extended data, supplementary information, acknowledgements, peer review information; details of author contributions and competing interests; and statements of data and code availability are available at https://doi.org/10.1038/s41586-020-2872-x.

1. Lorimer, D. R. et al. A bright millisecond radio burst of extragalactic origin. *Science* **318**, 777 (2007).
2. Petroff, E., Hessels, J. W. T. & Lorimer, D. R. Fast radio bursts. *Astron. Astrophys. Rev.* **27**, 4 (2019).
3. Lyubarsky, Y. A model for fast extragalactic radio bursts. *Mon. Not. R. Astron. Soc.* **442**, L9 (2014).
4. Beloborodov, A. M. A flaring magnetar in FRB 121102? *Astrophys. J. Lett.* **843**, 26 (2017).
5. Kaspi, V. M. & Beloborodov, A. M. Magnetars. *Annu. Rev. Astron. Astrophys.* **55**, 261 (2017).
6. Bochenek, C. D. et al. STARE2: detecting fast radio bursts in the Milky Way. *Publ. Astron. Soc. Pacif.* **132**, 034202 (2020).
7. Cordes, J. M., Bhat, N. D. R., Hankins, T. H., McLaughlin, M. A. & Kern, J. The brightest pulses in the Universe: multifrequency observations of the Crab pulsar's giant pulses. *Astrophys. J.* **612**, 375 (2004).
8. Marcote, B. et al. A repeating fast radio burst source localized to a nearby spiral galaxy. *Nature* **577**, 190–194 (2020).
9. Mereghetti, S. et al. INTEGRAL discovery of a burst with associated radio emission from the magnetar SGR 1935+2154. *Astrophys. J. Lett.* **898**, 29 (2020).
10. Ridnaia, A. et al. A peculiar hard X-ray counterpart of a Galactic fast radio burst. Preprint at https://arxiv.org/abs/2005.11178 (2020).
11. Li, C. K. et al. Identification of a non-thermal X-ray burst with the Galactic magnetar SGR J1935+2154 and a fast radio burst with Insight-HXMT. Preprint at https://arxiv.org/abs/2005.11071 (2020).
12. Metzger, B. D., Margalit, B. & Sironi, L. Fast radio bursts as synchrotron maser emission from decelerating relativistic blast waves. *Mon. Not. R. Astron. Soc.* **485**, 4091–4106 (2019).
13. Lyubarsky, Y. Fast radio bursts from reconnection in magnetar magnetosphere. *Astrophys. J.* **897**, 1 (2020).
14. Barthelmy, S. D. et al. Swift detection of multiple bursts from SGR J1935+2154. *GRB Circ. Netw.* **27657**, https://gcn.gsfc.nasa.gov/gcn3/27657.gcn3 (2020).
15. Scholz, P. et al. A bright millisecond-timescale radio burst from the direction of the Galactic magnetar SGR J1935+2154. *Astron. Telegr.* **13681**, http://www.astronomerstelegram.org/?read=13681 (2020).
16. Zhang, C. F. et al. A highly polarised radio burst detected from SGR J1935+2154 by FAST. *Astron. Telegr.* **13699**, http://www.astronomerstelegram.org/?read=13699 (2020).
17. Kothes, R., Sun, X., Gaensler, B. & Reich, W. A radio continuum and polarization study of SNR G57.2+0.8 associated with magnetar SGR J1935+2154. *Astrophys. J.* **852**, 54 (2018).
18. Zhou, P. et al. Revisiting the distance, environment and supernova properties of SNR G57.2+0.8 that hosts SGR J1935+2154. Preprint at https://arxiv.org/abs/2005.03517 (2020).
19. Kozlova, A. V. et al. The first observation of an intermediate flare from SGR J1935+2154. *Mon. Not. R. Astron. Soc.* **460**, 2008–2014 (2016).
20. Kuzmin, A. D. Giant pulses of pulsar radio emission. *Astrophys. Space Sci.* **308**, 563–567 (2007).
21. CHIME/FRB. A bright millisecond-duration radio burst from a Galactic magnetar. *Nature* http://doi.org/10.1038/s41586-020-2863-y (2020).
22. Sokolowski, M. et al. No low-frequency emission from extremely bright fast radio bursts. *Astrophys. J. Lett.* **867**, 12 (2018).
23. Bannister, K. et al. A single fast radio burst localized to a massive galaxy at cosmological distance. *Science* **365**, 565 (2019).
24. Ravi, V. et al. A fast radio burst localized to a massive galaxy. *Nature* **572**, 352–354 (2019).
25. Prochaska, J. X. et al. The low density and magnetization of a massive galaxy halo exposed by a fast radio burst. *Science* **366**, 231 (2019).
26. Macquart, J. P. et al. A census of baryons in the Universe from localized fast radio bursts. *Nature* **581**, 391–395 (2020).
27. Lu, W. & Kumar, P. On the radiation mechanism of repeating fast radio bursts. *Mon. Not. R. Astron. Soc.* **477**, 2470-2493 (2018).
28. Archibald, R. F., Kaspi, V. M., Tendulkar, S. P. & Scholz, P. The 2016 outburst of PSR J1119–6127: cooling and a spin-down-dominated glitch. *Astrophys. J.* **869**, 180 (2018).
29. Lu, W. & Piro, A. L. Implications from ASKAP fast radio burst statistics. *Astrophys. J.* **883**, 40 (2019).
30. Jarrett, T. H. et al. The WISE extended source catalog (WXSC). I. The 100 largest galaxies. Astrophys. *J. Suppl. Ser.* **245**, 25 (2019).
31. Manchester, R. N. & Taylor, J. H. *Pulsars* (W. H. Freeman, 1977).
32. Keane, E. F. The future of fast radio burst science. *Nat. Astron.* **2**, 865–872 (2018).
33. Villadsen, J. & Hallinan, G. Ultra-wideband detection of 22 coherent radio bursts on M dwarfs. *Astrophys. J.* **871**, 214 (2019).

Methods

The STARE2 instrument

STARE2 consists of a set of three radio receivers at locations across the southwestern United States. The receivers are located at the Owens Valley Radio Observatory (OVRO), the Goldstone Deep Space Communications Complex (GDSCC) and a site operated by the Telescope Array project[34] near Delta, Utah. Although the STARE2 receivers operate in the 1,280–1,530 MHz band, the useful band is limited to 1,280.732422–1,468.232422 MHz by radio frequency interference. STARE2 is sensitive to fast, dispersed radio transients above a detection threshold of $300(w)^{\frac{1}{2}}$ kJy, where w is the width of the burst (in units of milliseconds). STARE2 has a time resolution of 65.536 μs and a frequency resolution of 122.07 kHz. The instrument and data analysis are further described elsewhere[6]. Our station in Delta, Utah commenced operations after the publication of ref. [6]. With the addition of the third station, we now visually inspect candidate bursts if any pair of stations identifies a candidate event within 100 ms of each other.

STARE2 data consist of (a) candidate dispersed bursts that trigger the automated pipeline software and (b) spectra recorded every 65.536 μs with 2,048 frequency channels between 1,280 MHz and 1,530 MHz. The latter data span the full duration of the dispersion sweep of each candidate burst, with an additional 1,000 spectra both before and after the start and end of the dispersion sweep, respectively. Such time series of spectra are referred to as dynamic spectra. After de-dispersion, the available time series data on each burst span 131.072 ms, as displayed in Fig. 1 for FRB 200428.

To produce Fig. 1, the OVRO dynamic spectrum was smoothed with a two-dimensional boxcar function with a width of 0.524288 ms in time (equivalent to 8 bins) and 7.8125 MHz in frequency (equivalent to 64 bins). That is not the width of the pulse. We choose this smoothing timescale so that there is sufficient signal in each pixel to be visible. Data from the other stations were not summed for the purposes of display because of the different instrumental spectral responses, but they are shown in Extended Data Fig. 1. The data were baselined by subtracting the mean of the off-pulse region. We normalized the time series in each frequency bin by dividing by the standard deviation of the time series in each frequency bin, derived from the off-pulse region. The data were again normalized by the standard deviation of the off-pulse time and frequency bins to measure S/N in each time and frequency bin. To produce the time series, we simply took our dynamic spectra, which were processed as described above, averaged the data in frequency and re-normalized by the standard deviation of the time series in the off-pulse region.

Localization

To localize FRB 200428, we first measured the relative arrival times of the burst between each station. For this analysis, we used the frequency-averaged 65.536-μs-resolution total-intensity time series data. The data were de-dispersed with the DM that maximized S/N at OVRO. The time series was convolved with the boxcar function that maximized S/N at OVRO. These values were derived differently from those reported in the main text and thus differ slightly, as maximizing S/N rather than fitting the pulse profile to a model asks a different question of the data. The DM quantifies the observed frequency-dependent dispersion delay in terms of a free-electron column density. This DM and boxcar width were 333.3 pc cm^{-3} and 0.524288 ms, respectively. To measure S/N for this analysis, we take the frequency-averaged time series that has been de-dispersed and convolved with a boxcar function and subtract the mean of the off-pulse region. After this subtraction, the data are divided by the standard deviation of the time series in the off-pulse region. We measure $S/N = 21.6$ at OVRO, 15.7 at GDSCC and 20.1 at Delta. Data from each station are shown in Extended Data Fig. 1.

After determining S/N at each station and processing the data as described above, we then cross-correlate the time series from each pair of stations. We fit the peak of the correlation curve with a Lorentzian function. The location of the peak of the Lorentzian corresponds to the time delay between the two stations in the baseline. We find a time delay of −7 μs for OVRO-GDSCC, −884 μs for OVRO-Delta and −888 μs for GDSCC-Delta. The statistical uncertainty in the time delays is given by the boxcar width divided by the S/N of the station with the lowest S/N. For OVRO-GDSCC and GDSCC-Delta this uncertainty is 33 μs and for OVRO-Delta it is 26 μs.

To estimate the systematic uncertainty, we take advantage of a test of the Global Positioning System (GPS) L3 signal at 1,381 MHz on 28 February 2019. We recorded data with a time resolution of 131.072 μs during the test. Because the data were taken before the Delta station was built, this analysis was carried out only with OVRO and GDSCC. However, because we use an identical receiver and GPS timing hardware at the Delta station, we expect similar systematics to be present. During testing, the L3 signal turns on and off, enabling a test of the measured time delay between each station. The intrinsic time delay of the emission of the L3 signal between two satellites is expected to be of the order of microseconds, given that the GPS satellites are synchronized in transmission. Furthermore, the received signal is dominated by the satellites closest to zenith. At the time of the signal considered, the satellite expected to dominate the signal had an expected time delay of 46 μs between OVRO and GDSCC. This is less than the time resolution of our data. We measure the time delay as described above, except that in this analysis we only consider frequencies corresponding to the L3 signal and we do not convolve our time series with a boxcar function. We find a systematic uncertainty of 81 μs, which represents the measured time delay of the GPS L3 signal between OVRO and GDSCC.

To convert the measured time delays for FRB 200428 into a sky position, for each baseline we calculate the expected time delay for a given sky location over a fine grid in azimuth and elevation at a reference location. The reference location is chosen to be OVRO for the OVRO-GDSCC and OVRO-Delta baselines, whereas GDSCC is chosen for GDSCC-Delta. We then transform the grid of azimuths and elevations into right ascensions and declinations for the time of the burst. Then, the localization for one baseline is those sky positions that are consistent with the measured time delays and uncertainties. This corresponds to an arc across the sky for one baseline.

To combine the baselines, we assign a probability to each sky location for each arc assuming Gaussian statistical and systematic uncertainties, parameterized by the distance from the arc with no uncertainty. The mean of the Gaussian corresponds to the arc with no uncertainty and the standard deviation corresponds to the width of the arc assuming a 1σ uncertainty in the time delay. The probabilities for each arc and sky location are then multiplied together and normalized. We smooth the probability distribution with a two-dimensional Gaussian with a standard deviation of 1°. The transformation between local coordinate systems and the celestial coordinate system produces a sparse array of probabilities that requires smoothing to visualize. The smoothing radius is much smaller than the size of the localization region. This produces the probabilities shown in the right panel of Fig. 2 as arcs.

With these probabilities, we measured the 95% confidence interval of the STARE2 three-station localization region by modelling it as an ellipse. The 95% confidence interval corresponds to the smallest ellipse that encloses 95% of the probability distribution. To estimate this ellipse, we first determined the orientation of the ellipse. We measured the angle of the semi-major axis with respect to the declination axis by modelling the sky location probability distribution using a principal component analysis with two components. The angle of the semi-major axis corresponds to the angle of the eigenvector of the principal component with the highest eigenvalue; this angle is 57.88°. We calculated the expectation values of the right ascension and declination directly from their marginalized probability distributions. We found a right ascension of $\alpha = 19$ h 55 min ± 15° and a declination of $\delta = 14$ d ± 19°. The uncertainties contain 95% of the probability in each dimension

(95% localization). We then fitted the semi-major and semi-minor axes by minimizing the loss function $\mathcal{L}(a, b)$ in equation (1) using gradient descent. In equation (1), $p(\alpha', \delta')$ is the probability that the event occurred at that sky location, a is the semi-major axis, b is the semi-minor axis and λ is a regularization hyperparameter, which we set to 2.7×10^{-2}. This regularization corresponds to the ellipse area that contributes approximately equally to the loss as the confidence interval when $|\int_{\text{ellipse}} p(\alpha', \delta')\mathrm{d}\alpha'\mathrm{d}\delta' - 0.95| < 0.001$. We find $a = 12.3°$ and $b = 5.85°$. To derive the 68.4% and 90% confidence regions, we scale the ratio of the semi-major and semi-minor axes of the 95% confidence ellipse so that the appropriate amount of probability is contained.

$$\mathcal{L}(a, b) = \left(\int_{\text{ellipse}} p(\alpha', \delta')\mathrm{d}\alpha'\mathrm{d}\delta' - 0.95\right)^2 + \lambda ab. \quad (1)$$

Properties of FRB 200428

The dynamic spectrum of FRB 200428 was analysed using methods previously applied to FRBs detected by the Parkes telescope[35]. First, the dynamic spectra of FRB 200428 at the native time and frequency resolutions (65.536 μs and 122.07 kHz) obtained from OVRO and GDSCC were summed. No correction for the OVRO-GDSCC geometric arrival time delay was applied because the correction (−7 μs) is much smaller than the time resolution. Data from Delta were not included in the sum and in subsequent analysis, because of the increased presence of radio frequency interference at the Delta station (Extended Data Fig. 1). No calibrations were applied to the data, because none were available. After excising frequency ranges at the edges of the band that are always affected by radio frequency interference and are set to zero in the real-time pipeline (1,468.232422–1,529.267578 MHz and 1,279.267578–1,280.732422 MHz), we formed time series in four evenly spaced sub-bands after de-dispersing at an initial DM of 332.72 pc cm^{-3} (ref. [21]). The time series in each sub-band were normalized by the root-mean-square noise level in 50-ms intervals of data on either side of the burst. As described in ref. [35], we fitted a series of models with increasing complexity, stopping when the Bayes information criterion (BIC) did not favour the more complex models. We found that a model combining an intrinsic width in excess of the dispersion-smeared instrumental resolution, convolved with a one-sided exponential function with a characteristic timescale scaling as ν^{-4} (ν is the radio frequency) was negligibly preferrable according to a change in BIC of 1 unit. This corresponds to Model 3 of ref. [35] with $\alpha = 4$. The free parameters of the fit were the intrinsic width of the burst (assumed to be frequency-independent), a reference arrival time at 1,529.267578 MHz, a correction to the assumed DM, the 1/e timescale of the exponential function, and the burst fluences in each sub-band in data units. The convolution with the exponential is observed in several FRBs and radio pulsars, and is expected, owing to stochastic multi-path propagation of the burst due to refraction in inhomogeneous interstellar plasma[36]. This effect is commonly referred to as 'scattering'. Despite the insignificant evidence favouring the above model over a version with no scattering, we use this model because scattering was observed in the CHIME-detected event that was temporally coincident with FRB 200428 (ref. [21]).

The resulting best-fit burst parameters and the half-widths of their 68% confidence intervals are given in Table 1. The 1/e timescale of the scattering, scaled to a frequency of 1 GHz, as is common practise in the field[35], was 0.4(1) ms. The model fits in each sub-band are shown in Extended Data Fig. 2. The quoted band-averaged fluence (with an effective frequency of 1,378 MHz) was derived by averaging the fluences in each sub-band, and by scaling by the noise level according to the measured STARE2 system-equivalent flux density of 19 ± 2 MJy (ref. [6]) and the binning in frequency and time. An additional scaling of 1.33 was applied to correct for the location of the burst in the STARE2 primary beam, which was negligibly different at OVRO and GDSCC. The isotropic-equivalent energy release of FRB 200428 was calculated by scaling the fluence (in appropriate units) by $4\pi D^2 \nu_0$, where D is the distance to SGR 1935+2154 and ν_0 = 1,374.482422 MHz is the midpoint of the STARE2 band. This procedure was consistent throughout the paper.

The burst had an intrinsic width of 0.61(9) ms. As we do not coherently de-disperse our data, it is possible that there is unresolved structure to the burst. However, the intra-channel smearing timescale is 0.122 ms and the scattering timescale at 1.32 GHz is 0.312 ms (ref. [37]). This leads us to conclude that there is intrinsic structure throughout the 0.61(9)-ms burst.

The adopted distance to SGR 1935+2154 is consistent with the DM of FRB 200428. According to two models of the Galactic distribution of free electrons, this DM corresponds to distances of 6–13 kpc (ref. [38]) and 4–16 kpc (ref. [39]), respectively. However, the significant uncertainties in these models and in the distance to SGR 1935+2154 make it difficult to numerically constrain any potential DM excess associated with the SGR. The DMs in the two models corresponding to the lowest possible distance (6.6 kpc)[18] to SGR 1935+2154 are approximately 200 pc cm^{-3} (ref. [36]) and 190 pc cm^{-3} (ref. [38]). Thus, an approximate upper limit to any potential DM excess associated with SGR 1935+2154 is 140 pc cm^{-3}.

The analysis of the dynamic spectrum of the burst presented above provides a reference arrival time at 1,529.267578 MHz. This refers to the midpoint of the Gaussian function used to model the intrinsic burst structure. We note that it is unlikely that the burst is truly Gaussian in its intrinsic structure and that the presence of complex structure in the time–frequency plane (as is observed in some FRBs[40]) could bias this result at the approximately 0.1 ms level. The reference arrival time was converted to a UTC arrival time at OVRO using the recorded UTC of the first spectrum in the dataset. This time was converted to an arrival time at infinite frequency ($\nu = \infty$) using the fitted DM of 332.702(8) pc cm^{-3} and a dispersion constant of $(1/2.41) \times 10^4$ s MHz^2 pc^{-1} cm^3 (ref. [31]). The Earth centre arrival time was then calculated by adding a correction of 0.019210268 s to the OVRO arrival time. This correction was derived using the known position of the OVRO station and the v2.0 Astropy software package[41].

Searches for sub-threshold events from SGR 1935+2154

We searched the STARE2 data 65.536 ms before and after the burst for sub-threshold pulses at the same DM and widths of 0.066–4.194 ms at each station. We found no convincing candidates. Assuming that we would detect a burst with $S/N > 5$, we place a limit on the fluence of other bursts in this time range at <400 kJy ms. This fluence is obtained by scaling the measured fluence by the median S/N reported by our pipeline (18.3) divided by our sub-threshold search threshold of 5. We choose to use the median S/N reported by our pipeline because we require detections from two stations to claim that there is evidence for other pulses.

We detect only one component in FRB 200428, whereas the coincident CHIME event[21] consists of two components. We identify the second CHIME burst as the lower-freqency component to the STARE2 burst, because the geocentric arrival time at infinite frequency reported in Table 1 is consistent with that reported by the CHIME/FRB collaboration at 14:34:24.24.45547(2) on 28 April 2020 (ref. [21]). We place an upper limit on the L-band emission from the first CHIME component at 400 kJy ms.

Rate calculation

STARE2 had been observing for 448 days before FRB 200428. For the first 290 days, STARE2 observed only with its stations at OVRO and GDSCC. We observed with all three stations for 158 days before FRB 200428. Throughout this time, in addition to FRB 200428, we detected several solar radio bursts[6], but no other radio burst above a detection threshold of approximately 300 kJy ms$^{1/2}$.

To measure the all-sky rate of fast radio transients above the energy of FRB 200428, we first modelled the population of fast radio transients as a Poisson process. We then calculated our effective observing time for two epochs of observation. The first epoch corresponds to our two-station system, and the second epoch corresponds to our three-station system.

We used the single-station completeness reported in ref. [6] and an effective solid angle of 1.84 sr to convert our observing time into an effective observing time. The single-station completeness gives the two-station system a completeness of 0.56 and the three-station system a completeness of 0.95. The solid angle was chosen such that the median *S*/*N* reported by our detection pipeline (18.3) would be at the detection threshold of 7.3 at the edge of the solid angle. This gives the area for which a burst of this fluence would have been detected. Using these parameters, we estimated a total effective observing time of 0.468 yr.

We then computed the probability of the all-sky rate for rates in the range 0–40 $(4\pi\,\mathrm{sr})^{-1}\,\mathrm{yr}^{-1}$, given that we observed for 0.468 yr before we found a burst. We find the all-sky rate of fast radio transients above 1.5 MJy ms is $3.58^{+3.44}_{-2.03}\,(4\pi\,\mathrm{sr})^{-1}\mathrm{yr}^{-1}$. The reported uncertainties are 1σ.

To estimate the volumetric rate of this type of transient, we use the formalism developed in ref. [6], which converts the all-sky rate of transients in a particular galaxy into a volumetric rate. The key assumption in this formalism is that the transient linearly tracks star-formation activity. This is justified by the fact that magnetars are young objects and that this object is in the plane of the Milky Way and is associated with a supernova remnant[17]. Using our computed all-sky rate, a star-formation rate in the Milky Way of $(1.65 \pm 0.19)M_\odot\,\mathrm{yr}^{-1}$ (ref. [42]; $M_\odot$, mass of the Sun) and a volumetric star-formation rate of $1.95 \times 10^{-2}\,M_\odot\,\mathrm{Mpc}^{-3}\,\mathrm{yr}^{-1}$ (ref. [43]), we find that the volumetric rate of this type of transient is $7.23^{+8.78}_{-6.13} \times 10^7\,\mathrm{Gpc}^{-3}\,\mathrm{yr}^{-1}$. This is consistent with the rate inferred by making an alternative assumption that transients such as FRB 200428 track the stellar mass of their hosts. This volumetric rate is consistent with extrapolating the luminosity function derived from a sample of bright FRBs from the Australian Square Kilometre Array Pathfinder reported in ref. [29] down to the energy of this burst. The volumetric rate of this burst, along with the FRB luminosity function, is shown in Extended Data Fig. 3. We note that the uncertainties in the volumetric-rate extrapolation are extremely conservative, because they do not take into account the fact that the uncertainties in the parameters of this luminosity function are correlated. For a version of this plot that takes this into account, see ref. [44].

Using our measured volumetric rate, we can compare it to the volumetric rate derived for a sample of FRBs from the Australian Square Kilometer Array Pathfinder (ASKAP)[29]. This ASKAP rate is $10^{2.6\pm0.4}\,\mathrm{Gpc}^{-3}\,\mathrm{yr}^{-1}$ above $10^{32}\,\mathrm{erg\,Hz}^{-1}$. We fit these two data points to the model given in equation (2), where $\Phi_{\mathrm{FRB}}(>E)$ is the volumetric rate of FRBs with energy greater than E, α is the slope of the luminosity function of FRBs and ϕ_0 is the volumetric rate of FRBs with $E > 10^{32}\,\mathrm{erg\,Hz}^{-1}$.

$$\log[\Phi_{\mathrm{FRB}}(>E)] = \alpha(\log E - 32) + \phi_0 \quad (2)$$

We assumed a uniform prior for ϕ_0 and α and a Poisson likelihood on the STARE2 rate, and used the posterior distribution from ref. [29] as the likelihood of the ASKAP rate. We find $\alpha = -0.91^{+0.09}_{-0.06}$ and $\phi_0 = 2.76^{+0.39}_{-0.17}$, where the uncertainties correspond to the 1σ confidence interval.

STARE2 limits on other X-ray bursts from SGR 1935+2154

We looked through our metadata of candidate events triggered by a single station for possible missed triggers coincident with previously reported flares from SGR 1935+2154. Our candidate metadata consist of *S*/*N* ratios, arrival times, DMs, pulse widths and the number of DM, pulse width and time trials that are consistent with being from the same candidate. We searched the metadata for candidates within 1 min of reported X-ray bursts from SGR 1935+2154 and that had an elevation angle >25° at OVRO at the time of the burst. We also restricted our search to candidates with DMs between 325 pc cm^{-3} and 340 pc cm^{-3}. We note that SGR 1935+2154 was the only SGR with known X-ray bursts that were visible to STARE2. We found no candidate events other than FRB 200428 that fit these criteria at any of the three STARE2 stations.

Given our single-station completeness of 0.74 (ref. [6]), our completeness for this analysis is expected to be approximately 0.93 for our two-station system and 0.98 for our three-station system. Our three-station system came online on MJD 58809, and thus only observed the X-ray bursts in MJD 58966–58987 (MJD, Modified Julian date).

We used our measured system-equivalent flux density, a typical observing bandwidth of 188 MHz and a threshold *S*/*N* of 7.3 to compute an upper limit on millisecond-duration radio transients for each event. We also applied a beam correction for each upper limit corresponding to the position of SGR 1935+2154 at OVRO. Our limits are shown in Extended Data Fig. 4. We include FRB 200428 as a blue dot. We also show our results and the list of X-ray bursts in Extended Data Table 1.

Data availability

Data are available upon request. These data are in a public archive by the Caltech Library at http://doi.org/10.22002/D1.1647 .

Code availability

Custom code is available at https://github.com/cbochenek/STARE2-analysis. The code used to fit the burst profiles is available on request.

34. Kawai, H. et al. Telescope array experiment. *Nucl. Phys. B* **175/176**, 221–226 (2008).
35. Ravi, V. The observed properties of fast radio bursts. *Mon. Not. R. Astron. Soc.* **482**, 1966–1978 (2019).
36. Cordes, J. M. & Chatterjee, S. Fast radio bursts: an extragalactic enigma. *Annu. Rev. Astron. Astrophys.* **57**, 417 (2019).
37. Kirsten, R. Detection of two bright FRB-like radio bursts from magnetar SGR J1935+2154 during a multi-frequency monitoring campaign. Preprint at https://arxiv.org/abs/2007.05101 (2020).
38. Yao, J. M., Manchester, R. N. & Wang, N. A new electron-density model for estimation of pulsar and FRB distances. *Astrophys. J.* **835**, 29 (2017).
39. Cordes, J. M. & Lazio, T. J. W. NE2001. I. A new model for the Galactic distribution of free electrons and its fluctuations. Preprint at http://arxiv.org/abs/astroph/0207156 (2002).
40. Hessels, J. W. T. et al. FRB 121102 bursts show complex time-frequency structure. *Astrophys. J.* **876**, L23 (2019).
41. Astropy Collaboration et al. The Astropy project: building an open-science project and status of the v2.0 core package. *Astron. J.* **156**, 123 (2018).
42. Licquia, T. C. & Newman, J. A. Improved estimates of the Milky Way's stellar mass and star formation rate from hierarchical Bayesian meta-analysis. *Astrophys. J.* **806**, 96 (2015).
43. Salim, S. et al. UV star formation rates in the local Universe. *Astrophys. J. Suppl. Ser.* **173**, 267 (2007).
44. Lu, W. et al. A unified picture of Galactic and cosmological fast radio bursts. *Mon. Not. R. Astron. Soc.* **498**, 1397–1405 (2020).

Acknowledgements We thank the then director of OVRO, A. Readhead, for funds (derived from the Alan Moffet Funds) that allowed us to start this project. The Caltech and Jet Propulsion Laboratory President's and Director's Fund enabled us to build the second system at Goldstone and the third system near Delta, Utah. We are thankful to Caltech and the Jet Propulsion Laboratories for the second round of funding. C.D.B., a PhD student, was partially supported by the Heising-Simons foundation. We also thank S. Weinreb and D. Hodge for building the front-end and back-end boxes, J. Lagrange for support at GDSCC, J. Matthews and the Telescope Array Collaboration for assistance at Delta, and the entire OVRO staff, in particular J. Lamb, D. Woody and M. Catha, for support. We thank S. Phinney and W. Lu for comments on the manuscript. A portion of this research was performed at the Jet Propulsion Laboratory, California Institute of Technology, under a contract with the National Aeronautics and Space Administration. This research was additionally supported by the National Science Foundation under grant AST-1836018. This research made use of Astropy, a community-developed core Python package for Astronomy. This research also used the SIMBAD database, operated at CDS, Strasbourg, France.

Author contributions S.R.K., C.D.B., D.L.M., V.R., K.V.B. and G.H. conceived and developed the STARE2 concept and observing strategy. C.D.B., D.L.M., K.V.B., J.K. and S.R.K. led the construction and initial deployment of STARE2. C.D.B., D.L.M., K.V.B., V.R., J.K. and G.H. designed and built the STARE2 subsystems. C.D.B., D.L.M. and K.V.B. commissioned STARE2. C.D.B. operated STARE2, performed the localization and transient rate analyses, as well as the searches for sub-threshold events and events associated with other SGR flares. V.R. extracted the properties of the burst. C.D.B. and V.R. led the writing of the manuscript with the assistance of all co-authors.

Competing interests The authors declare no competing interests.

Additional information
Correspondence and requests for materials should be addressed to C.D.B.
Peer review information *Nature* thanks Evan Keane and Amanda Weltman for their contribution to the peer review of this work.

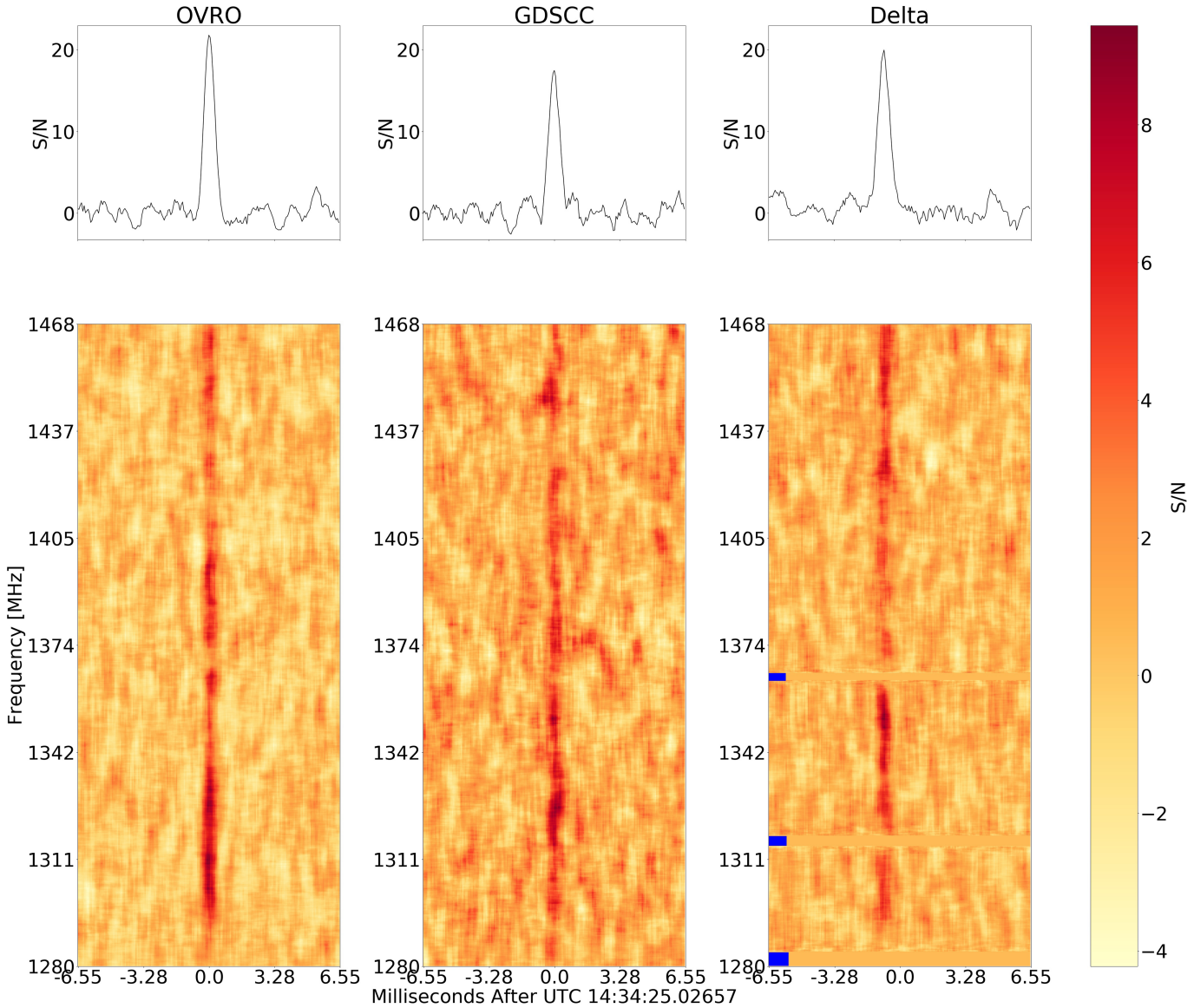

Extended Data Fig. 1 | Time series and dynamic spectrum of FRB 200428 at each station. Top, time series at each station referenced to the arrival time at OVRO at $\nu = 1{,}529.267578$ MHz. Bottom, dynamic spectra at each station. The data shown in all panels were processed in the same way as those in Fig. 1. We have not corrected for the spectral response at each station. The blue bars in the Delta dynamic spectrum indicate frequencies affected by radio frequency interference that were excised from the data.

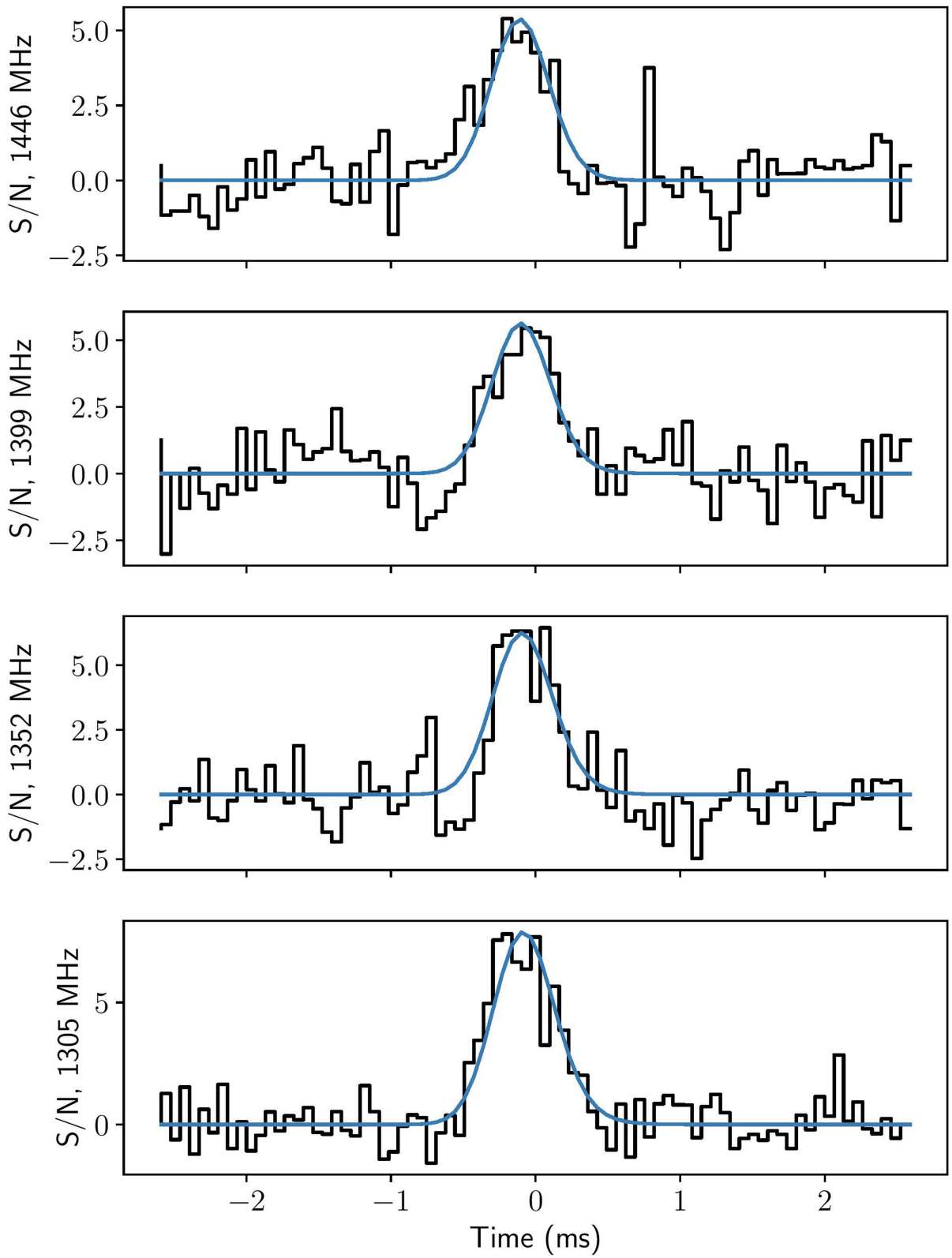

Extended Data Fig. 2 | Fits to data on FRB 200428 in four sub-bands. Black lines indicate the raw data and blue lines show the best-fit model. The sub-band centre frequencies are indicated beside each plot.

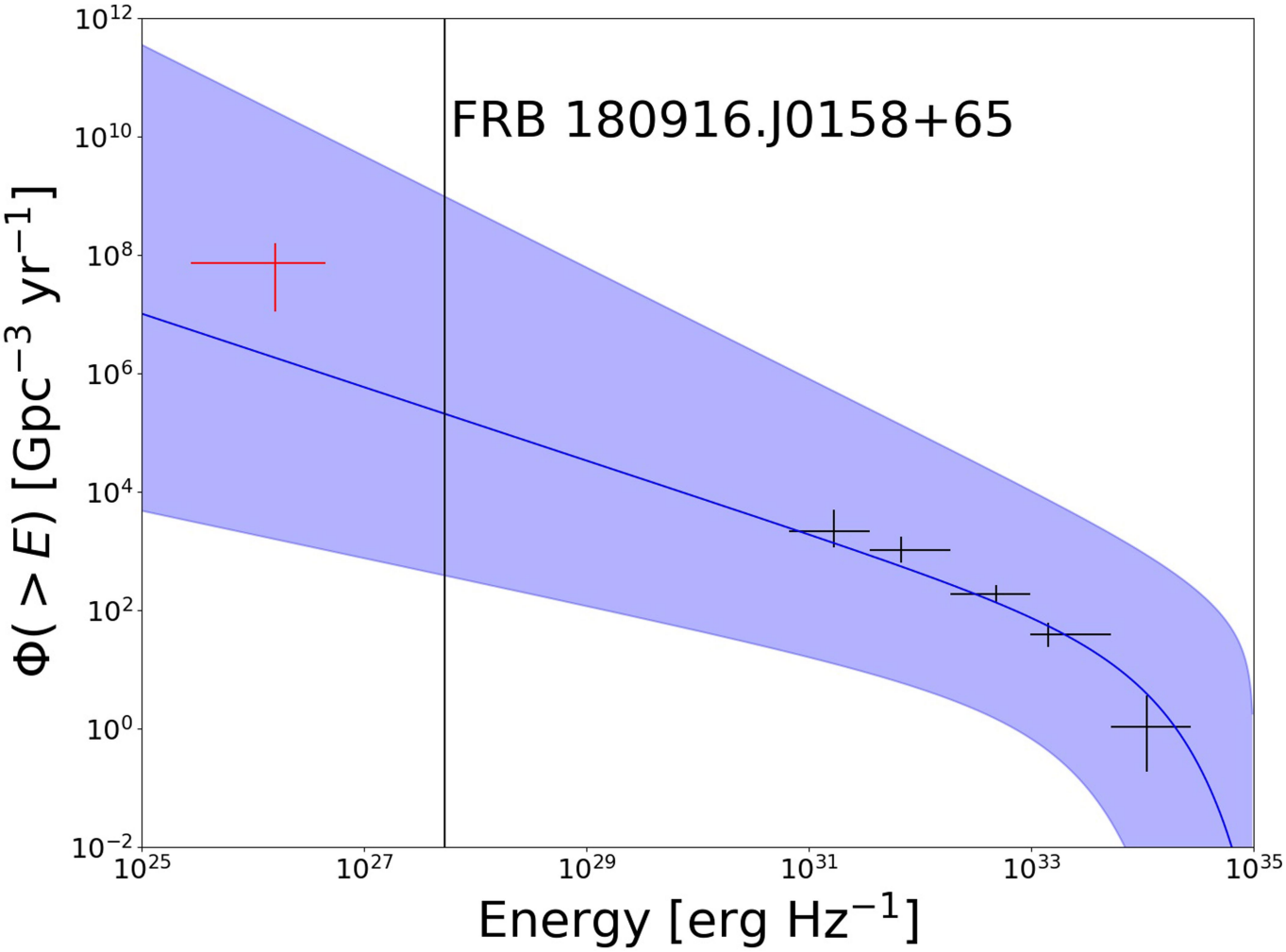

Extended Data Fig. 3 | Volumetric rates of FRBs. Volumetric rate, $\Phi(>E)$, calculated from the radio burst from SGR 1935+2154 (red cross) compared with the extrapolated luminosity function of bright FRBs[29] (blue-shaded region). The black crosses represent the volumetric rate of FRBs determined from the ASKAP Fly's Eye sample[29]. We note that correlated probabilities between the parameters of the luminosity function are not taken into account, leading to an overestimate of the uncertainty in the blue-shaded region; see ref. [43] for a similar plot in which they are taken into account. The volumetric rate was calculated by modelling the population of Galactic fast radio transients as a Poisson process and assuming that these fast radio transients track star formation. The uncertainties on this measurement are 1σ statistical uncertainties, in addition to the maximum range of possible distances to SGR 1935+2154 (4–16 kpc)[39]. We also show the energy of the weakest burst detected from FRB 180916.J0158+65—a repeating FRB—for comparison[8]. The volumetric rate of Galactic fast radio transients is consistent with extrapolating the luminosity function of bright FRBs to the energy of FRB 200428.

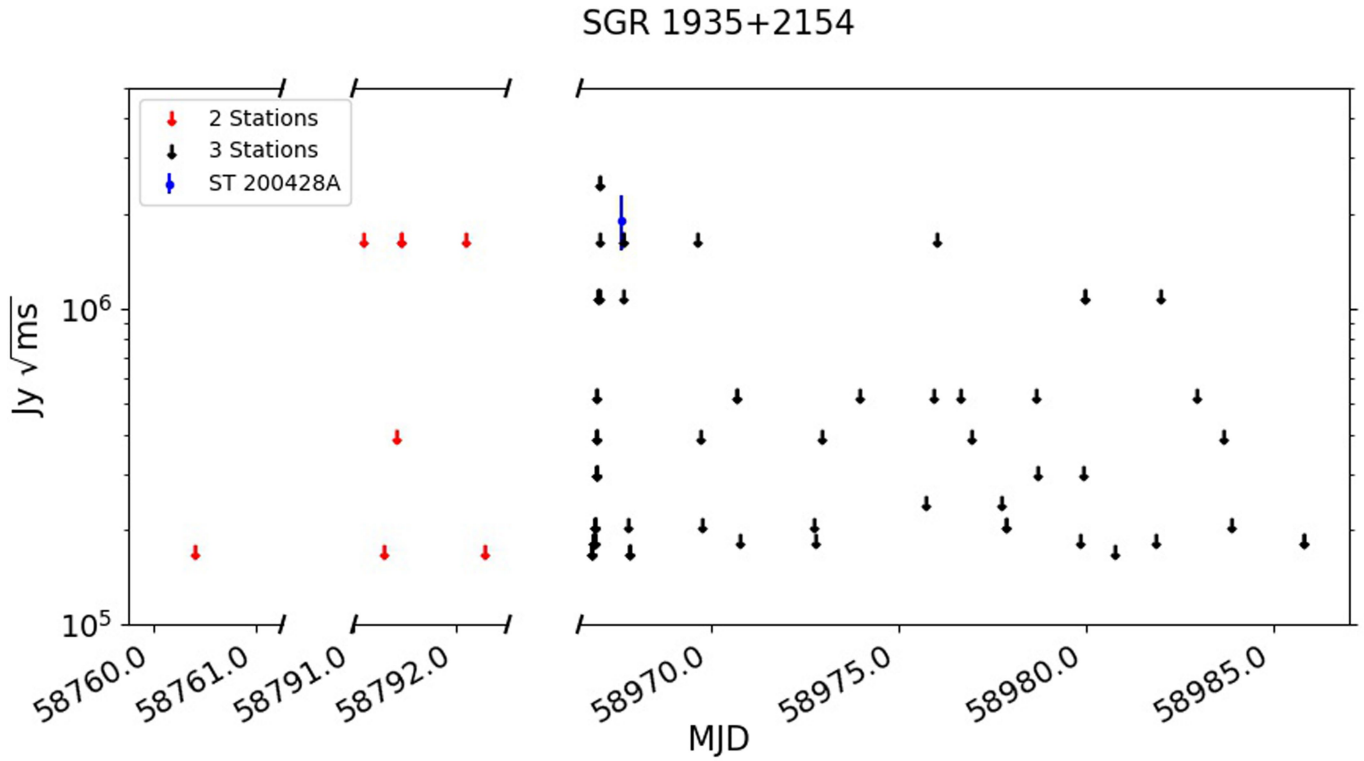

Extended Data Fig. 4 | Upper limits on fast radio transients from other flares of SGR 1935+2154 observable by STARE2. The ordinate shows the 7.3σ upper limit on the fluence of a potential burst in Jy ms$^{1/2}$, and the abscissa shows the times (in MJD) of reported flares from SGR 1935+2154. The derivation of the upper limits is described in Methods. We note that our three-station system was observing only during the flares between MJD 58966 and MJD 58987, shown in black. For the other flares, only our stations at OVRO and GDSCC were observing, shown in red. We show FRB 200428 in blue; the error bar represents the standard error in the measured fluence.

Extended Data Table 1 | STARE2 7.3σ upper limits on reported X-ray bursts from SGR 1935+2154 that occurred in the STARE2 field of view

MJD	OVRO Elevation	Limit (MJy $\sqrt{\text{ms}}$)[a]	Citation[b]
58791.44753023148	32°	1.65	GCN 26242
58792.257743055554	75°	0.17	GCN 26242
58792.06695601852	29°	1.65	GCN 26171
58791.07959490741	31°	1.65	GCN 26169
58791.44752314815	32°	1.65	GCN 26160
58791.38741898148	49°	0.39	GCN 26160
58791.27361111111	74°	0.17	GCN 26153
58760.375621527775	73°	0.17	GCN 25975
58967.77195601852	75°	0.17	GCN 27667
58966.822041064814	71°	0.18	GCN 27667
58966.91622886574	46°	0.53	GCN 27667
58966.98925520833	25°	2.51	GCN 27667
58966.76828703703	74°	0.17	ATel 13675, GCN 27689
58966.77290509259	74°	0.17	GCN 27664
58966.843981481485	66°	0.21	GCN 27664
58966.77222222222	74°	0.17	GCN 27663
58966.78204861111	75°	0.17	GCN 27663
58966.97083333333	30°	1.65	GCN 27663
58966.83456018518	68°	0.18	GCN 27661, ATEL 13748
58966.91392361111	47°	0.53	GCN 27661
58966.82204861111	71°	0.18	ATEL 13748
58966.822916666664	70°	0.18	ATEL 13748
58966.83023148148	69°	0.18	ATEL 13748
58966.83445601852	68°	0.18	ATEL 13748
58966.838425925926	67°	0.21	ATEL 13748
58966.84224537037	66°	0.21	ATEL 13748
58966.84280092592	66°	0.21	ATEL 13748
58966.84364583333	66°	0.21	ATEL 13748
58966.87943287037	56°	0.3	ATEL 13748
58966.885243055556	55°	0.3	ATEL 13748
58966.885833333334	55°	0.3	ATEL 13748
58966.88952546296	54°	0.3	ATEL 13748
58966.892372685186	53°	0.3	ATEL 13748
58966.893599537034	52°	0.39	ATEL 13748
58966.903275462966	50°	0.39	ATEL 13748
58966.90493055555	49°	0.39	ATEL 13748
58966.946388888886	37°	1.1	ATEL 13748
58966.94936342593	37°	1.1	ATEL 13748
58966.955092592594	35°	1.1	ATEL 13748
58966.960335648146	33°	1.1	ATEL 13748

[a]The upper limits represent a threshold *S/N* of 7.3σ.

[b]'GCN' refers to *GRB Circular Network* and "ATEL" refers to *The Astronomer's Telegram*.

Extended Data Table 2 | STARE2 7.3σ upper limits on reported X-ray bursts from SGR 1935+2154 that occurred in the STARE2 field of view

MJD	OVRO Elevation	Limit (MJy $\sqrt{\text{ms}}$)[a]	Citation[b]
58966.987974537034	26°	2.51	ATEL 13748
58985.758935185186	72°	0.18	ATEL 13748
58967.59783008102	32°	1.65	ATEL 13729
58967.59789236111	32°	1.65	ATEL 13729
58967.60722395833	35°	1.1	ATEL 13729
58967.71905366898	66°	0.21	ATEL 13729
58967.792013287035	74°	0.17	ATEL 13729
58967.79305381944	74°	0.17	ATEL 13729
58969.58160091435	29°	1.65	ATEL 13729
58969.6540966088	50°	0.39	ATEL 13729
58969.717278206015	66°	0.21	ATEL 13729
58970.629127719905	43°	0.53	ATEL 13729
58970.635658287036	45°	0.53	ATEL 13729
58970.72921851852	70°	0.18	ATEL 13729
58972.70829861111	66°	0.21	ATEL 13729
58972.71731018519	68°	0.18	ATEL 13729
58972.88183449074	51°	0.39	ATEL 13729
58973.90270061343	44°	0.53	ATEL 13729
58975.67770486111	61°	0.24	ATEL 13729
58975.89255034722	46°	0.53	ATEL 13729
58975.950249421294	29°	1.65	ATEL 13729
58976.61089872685	43°	0.53	ATEL 13729
58976.87895075232	49°	0.39	ATEL 13729
58977.662045833335	58°	0.24	ATEL 13729
58977.80805587963	67°	0.21	ATEL 13729
58977.81765358796	65°	0.21	ATEL 13729
58978.61405034722	45°	0.53	ATEL 13729
58978.648174884256	55°	0.3	ATEL 13729
58979.78681759259	70°	0.18	ATEL 13729
58979.84469907408	56°	0.3	ATEL 13729
58979.91060440972	37°	1.1	ATEL 13729
58979.922326388885	34°	1.1	ATEL 13729
58980.71925138889	73°	0.17	ATEL 13729
58981.786238113425	69°	0.18	ATEL 13729
58981.90814050926	37°	1.1	ATEL 13729
58982.883207824074	43°	0.53	ATEL 13729
58983.61761574074	50°	0.39	ATEL 13729
58983.810202037035	63°	0.21	ATEL 13729
58985.75893611111	72°	0.18	ATEL 13729

[a]The upper limits represent a threshold *S/N* of 7.3σ.
[b]'ATEL' refers to *The Astronomer's Telegram*.